Ion-Pair Theory of Concentrated Electrolytes. II. Approximate Dielectric Response Calculation

RONALD LOVETT* AND FRANK H. STILLINGER, JR.
Bell Telephone Laboratories, Incorporated, Murray Hill, New Jersey

(Received 11 January 1968)

The theoretical program initiated in the preceding paper is continued. The wavelength-dependent dielectric response function for the "primitive-model" electrolyte, $\epsilon(k)$, is evaluated by means of a self-consistent torque calculation for ion pairs in an external field. The result is used to obtain the longest-ranged component of the ion-atmosphere charge density. The rigorous second-moment condition on the ion atmosphere then is used to compute crudely the short-ranged components. Besides the usual low-concentration terms, the implied free energy [Eq. (76)] and activity coefficient [Eq. (77)] contain negative terms varying with the four-thirds power of concentration.

I. INTRODUCTION

The preceding Paper I[1] provides an alternative to the usual means of describing electrolytes in terms of ionic distribution functions. Its strategy of pairing all ions converts the electrolyte to a fluid of "dipolar molecules" of variable length, and invites introduction of a wavelength-dependent dielectric response function, $\epsilon(k)$.

The quantity $\epsilon(k)$ expresses the ability of the electrolyte to shield the various Fourier components of a weak, externally applied electrostatic potential. Some fundamental and important connections were established in Paper I, Sec. III, between $\epsilon(k)$ and conventional ionic-pair distribution functions on the one hand, and between $\epsilon(k)$ and "dipolar molecule" pair distribution functions on the other hand. Since it is our major objective to construct a new approach to understanding electrolytes, we offer below a calculation of $\epsilon(k)$, albeit an approximate one, which does not explicitly require knowledge of either class of pair distribution functions. The result may be used, though, to make an independent prediction about the nature of ion-atmosphere charge distribution.

As in Paper I, primary concern centers about the "primitive-model" electrolyte; that is, the ions are regarded as rigid spheres all of diameter a suspended in an ideal dielectric medium, and they all bear charges $\pm Ze$. Even with this restriction the analysis is far from trivial, so it is carried out in several stages of ascending complication.

The first stage is contained in Sec. II below. There, attention is focused on the formal particle-pairing process for a binary mixture of point particles without interactions. Although at first sight it may seem odd to devote any effort to description of an ideal gas mixture when the very essence of the concentrated electrolyte of interest is strong (and long-ranged!) interactions, the corresponding "dipolar molecule" size distribution function $p^{(1)}(s)$ provides valuable guides for the more complicated cases. A nonlinear integral equation for $p^{(1)}(s)$ is obtained, and its solution compared with a Monte Carlo pairing "experimental" determination of the ideal gas $p^{(1)}(s)$. The most important observation, perhaps, is that $p^{(1)}(s)$ possesses a characteristic s^{-6} tail for large size s.

Section III takes up the next stage of complication, the pairing process for a binary mixture of geometrically identical rigid spheres (essentially a discharged "primitive-model" electrolyte). Because of the rigorous rigid-sphere exclusion, the distribution $p^{(1)}(s)$ vanishes for $s<a$, but the existence of a small $(s-a)$ development of $p^{(1)}(s)$ for $s>a$ is demonstrated. It is furthermore argued that the s^{-6} tail persists upon introduction of rigid-sphere interactions.

It was shown in Paper I that the particle pairing process generates strong "steric-hindrance" interactions between dipolar molecules, that must be reckoned with even for the binary ideal-gas case. Section IV provides a key observation that permits circumvention of these complicated steric-hindrance effects in an approximate evaluation of $\epsilon(k)$. It is shown that these effects may be disregarded (i.e., dipolar molecules treated as rotating independently) in calculating system linear response to an external field *provided* that a wavelength-dependent renormalization constant $\lambda(k)$ is used to readjust appropriately the external field strength. The explicit construction of $\lambda(k)$ shows it to be a functional of $p^{(1)}(s)$.

In the light of this observation, Sec. V proceeds to develop a self-consistent computation for $\epsilon(k)$. The dipolar molecules formed from the primitive-model ions will tend to reorient in the presence of an external, sinusoidal electrostatic potential so as to produce a mean sinusoidal charge density. The field tending to orient the dipolar molecules is then the combination of the external plus induced fields, and in accord with the remarks of Sec. IV, their sum is renormalized with $\lambda(k)$.

The resulting $\epsilon(k)$ is applied to determination of the electrolyte free energy in Sec. VI. In order to minimize errors arising from approximations in the $\epsilon(k)$ calculation, the ion-atmosphere second-moment condition derived in Paper I is employed. The free-energy and

* Present address: Department of Chemistry, Washington University, St. Louis, Mo. 63130.

[1] F. H. Stillinger, Jr., and R. Lovett, J. Chem. Phys. **48**, 3858 1968, preceding article.

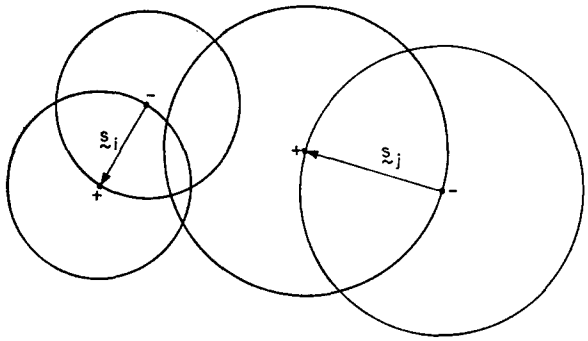

FIG. 1. Spherical envelopes, for pairs i and j of noninteracting point particles, associated with steric hindrance potential $u(\mathbf{x}_i, \mathbf{x}_j)$. The configuration shown is "allowed", i.e., $u=0$.

activity-coefficient results exhibit contributions varying as the four-thirds power of electrolyte concentration, which seem not to have been found in earlier electrolyte work.

A final discussion Sec. VII indicates possible routes for extension of our approach, including a variational procedure that may prove useful for molten salts. Also, Appendices are included concerning (a) an approximate integral relation satisfied by the ideal gas $p^{(1)}(s)$, and (b) roots of a characteristic transcendental equation that arises in the theory both here and elsewhere.[2-4]

II. PAIRING IN IDEAL GASES

Into a container of macroscopic volume V we will place at random a large number N of each of two types of point particles. In view of our ultimate goal the two species of particles will be identified by the symbols $-$ and $+$. For convenience we now respecify the complete pairing process advocated in Paper I.

(a) From the entire set of distances between pairs of points of opposite species choose the smallest,[5] and consider the two points involved to be paired.

(b) Examine next the distances between unlike pairs only for the remainder set of $2N-2$ particles, and again pair off the $-$ and $+$ particles which are closest in this reduced set.

(c) Continue the process of pairing the closest $-$, $+$ duo in whatever set of unpaired particles remain at that stage, until all particles have been paired.

The end result is that each $-$ particle has one and only one $+$ partner, and vice versa. Our problem in this section is determination of the size distribution function for the pairs, in the infinite system size limit, N/V held fixed.

The configuration of the jth pair is described by a six-component vector $\mathbf{x}_j=\mathbf{R}_j\oplus\mathbf{s}_j$, comprising the position $\mathbf{R}_j$ of the center of the bond between the two particles, and the $-$ to $+$ vector separation, $\mathbf{s}_j$. In precise terms, $p^{(1)}(\mathbf{x})d\mathbf{x}$ will be the mean number of pairs in configuration element $d\mathbf{x}$. For determination of $p^{(1)}(\mathbf{x})$ we shall rely upon Eq. (22) in Paper I, transcribed suitably for the present ideal-gas case,

$$p^{(1)}(\mathbf{x}_1)=(N/V)^2\exp[-\beta W_c(\mathbf{x}_1)],$$
$$\beta=(k_BT)^{-1}. \tag{1}$$

The quantity $W_c(\mathbf{x}_1)$ was previously identified as a cavity free energy associated with the "steric-hindrance" potentials $u(\mathbf{x}_i, \mathbf{x}_j)$ that must be designated as acting between each pair ij of dipolar molecules.

Figure 1 presents a convenient pictorial device for presentation of the nature of $u(\mathbf{x}_i, \mathbf{x}_j)$ in the binary ideal-gas case. One first imagines that spheres are drawn about both ends of every pair, with radii equal to the pair's separation s_i. Then for the two pairs i and j, $u(\mathbf{x}_i, \mathbf{x}_j)$ is zero *unless* either of the distances between unlike ends of the two pairs is less than the smaller of s_i and s_j, in which case $u=+\infty$. In the terms of Fig. 1, where $s_i<s_j$, this means that the two pairs are free to move relative to one another, except that j's $+$ end cannot penetrate the sphere around i's $-$ end, and j's $-$ end cannot penetrate the sphere around i's $+$ end.

Cavity free energy $W_c(\mathbf{x}_1)$ in Eq. (1) thus has its genesis in the set of u's operative in the system. If the $\mathbf{s}_1$ component of $\mathbf{x}_1$ is very small, the existence of a pair at $\mathbf{x}_1$ clearly implies virtually no steric hindrance for the surrounding pairs; the cavity around $\mathbf{x}_1$ that must be devoid of other pairs in order validly to contain the postulated one will be likewise very small and easy to form (small free energy W_c required). At the other extreme of very large $\mathbf{s}_1$, the resulting very large cavity will require a very large reversible work W_c to create.

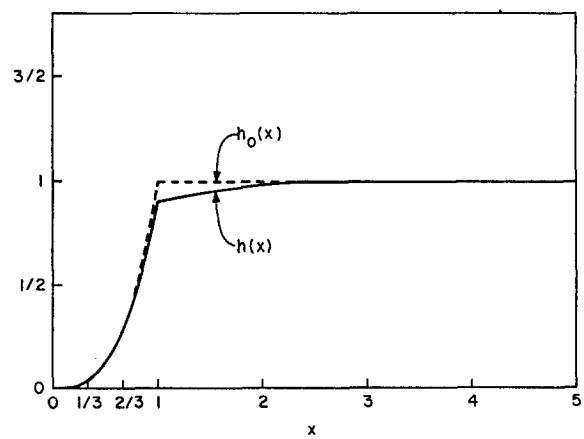

FIG. 2. Plot of $h(x)$ occurring in the size distribution integral Eq. (9) for the binary ideal-gas case, and of $h_0(x)$ in modified integral Eq. (14).

[2] J. G. Kirkwood and J. C. Poirier, J. Phys. Chem. **58**, 591 (1954).
[3] F. H. Stillinger, Jr., and J. G. Kirkwood, J. Chem. Phys. **33**, 1282 (1960).
[4] V. S. Krylov and V. G. Levitch, Zh. Fiz. Khim. **37**, 106 (1963).
[5] Accidental equality of two or more distances carries zero statistical weight and may be disregarded.

A cluster expansion for $W_c(\mathbf{x}_1)$ was displayed in Eq. (21) of Paper I, but as is always the case with such formal complete expansions, analytic intractability prevents general utility. In this section, however, we shall proceed by truncating the series after its first term, the binary pair cluster. In this approximation, Eq. (1) adopts the following form:

$$p^{(1)}(\mathbf{x}_1) = \left(\frac{N}{V}\right)^2 \exp\left(\int d\mathbf{x}_2 S^{(1)}(\mathbf{x}_1, \mathbf{x}_2)\, p^{(1)}(\mathbf{x}_2)\right); \quad (2)$$

$$S^{(1)}(\mathbf{x}_1, \mathbf{x}_2) = \exp[-\beta u(\mathbf{x}_1, \mathbf{x}_2)] - 1. \quad (3)$$

The nonlinear integral equation (2) has at least the virtue of sufficient simplicity that a solution may numerically be constructed without undue effort. Simplicity alone, however, is hardly adequate justification for drawing conclusions about the nature of the actual particle-pair size distribution. The important point to note though is that Eq. (2) is qualitatively correct in both the small-$\mathbf{s}_1$ and large-$\mathbf{s}_1$ limits, since the relevant cavity is principally outlined by the geometric extension of the hindrance potential $u(\mathbf{x}_1, \mathbf{x}_2)$. We therefore proceed under the presumption that Eq. (2) correctly retains the physical essence of the exact problem.[6]

The kernel $S^{(1)}$ manifests translational and rotational invariances that insure the intuitively obvious dependence of $p^{(1)}(\mathbf{x}_1)$ only on $|\mathbf{s}_1|$. From Eq. (3) we see furthermore that $S^{(1)}$ is nonvanishing only for the forbidden configurations $\mathbf{x}_1$, $\mathbf{x}_2$ for which $u(\mathbf{x}_1, \mathbf{x}_2)$ is infinite. For these reasons it is permissible to rewrite Eq. (2) thus,

$$p^{(1)}(s_1) = \left(\frac{N}{V}\right)^2 \exp\left(-\int_0^\infty \omega(s_1, s_2)\, p^{(1)}(s_2)\, ds_2\right), \quad (4)$$

in which $\omega(s_1, s_2)$ is the five-dimensional overlap volume described by u, for a fixed pair of constant separation s_1, and a movable one of constant separation s_2.

The actual calculation of $\omega(s_1, s_2)$ requires a great deal of petty geometry and trigonometry, whose reproduction here would serve no useful purpose. Therefore we merely quote the result:

$$\omega(s_1, s_2) = (32\pi^2/3) s_1^3 s_2^2 h(s_2/s_1); \quad (5)$$

$$\begin{aligned} h(x) &= x^3 && (0 \le x \le \tfrac{1}{3}), \\ &= (1/64)\{8x^2[4-3(1-x)^2] + 4x[8x^3-(1-x)^3] + (1/5x)[(1-x)^5 - 32x^5]\} && (\tfrac{1}{3} \le x \le 1), \\ &= (1/64x)\{8[4x^2-3(x-1)^2] + 4[8-(x-1)^3] + \tfrac{1}{5}[(x-1)^5 - 32]\} && (1 \le x \le 3), \\ &= 1 && (3 \le x < \infty). \end{aligned} \quad (6)$$

The piecewise rational function $h(x)$ has the property

$$x^{3/2} h(1/x) = x^{-3/2} h(x); \quad (7)$$

furthermore it is continuous, and is a nondecreasing function for $x > 0$. It is presented graphically in Fig. 2.

Set

$$p^{(1)}(s_1) = (N/V)^2 y(s),$$
$$s = (N/V)^{1/3} s_1. \quad (8)$$

The nonlinear integral equation (4) thereupon may be transformed to eliminate any explicit occurrence of density,

$$y(s) = \exp\left[-\left(\frac{32\pi^2}{3}\right) s^6 \int_0^\infty x^2 h(x)\, y(sx)\, dx\right]. \quad (9)$$

In view of its meaning as a probability, the solution $y(s)$ must be nonnegative, and integrable; specifically one should require

$$1 = 4\pi \int_0^\infty s^2 y(s)\, ds, \quad (10)$$

since from definitions (8) this is the requirement that any given particle be bonded at some distance to precisely one other particle. By virtue of the approximate nature of the binary-cluster truncation applied to the full nonlinear $p^{(1)}$ equation, one should not expect condition (10) still to be precisely obeyed. The deviation indeed could serve as an error indicator in our procedure.

Since our understanding of the operation of steric hindrance effects indicates that very large pairs should be very improbable, we anticipate that even the approximate $s^2 y(s)$ should decay to zero rather rapidly at large s. Suppose initially that $y(s)$ can be bounded above by an *exponentially* decaying function of s as $s \to +\infty$. Then for large enough s, the $y(sx)$ integrand factor will decay so fast to zero with increasing x that for all practical purposes only the first functional form of $h(x)$ in Eq. (9), x^3, need be considered. The integral in Eq. (9) then is as follows:

$$\int_0^\infty x^5 y(sx)\, dx = s^{-6} \int_0^\infty (x')^5 y(x')\, dx'. \quad (11)$$

After this result is inserted in Eq. (9), the conclusion is that $y(s)$ approaches a positive constant at large s. Not only is this physically absurd, but it contradicts the exponential decay hypothesis.

[6] The appropriateness of the binary-cluster approximation used here should be judged in the light of its success in explaining completely different phenomena; with regard to liquid crystals (where steric hindrances are also of paramount importance) see: L. Onsager, Ann. N.Y. Acad. Sci. **51**, 627 (1949).

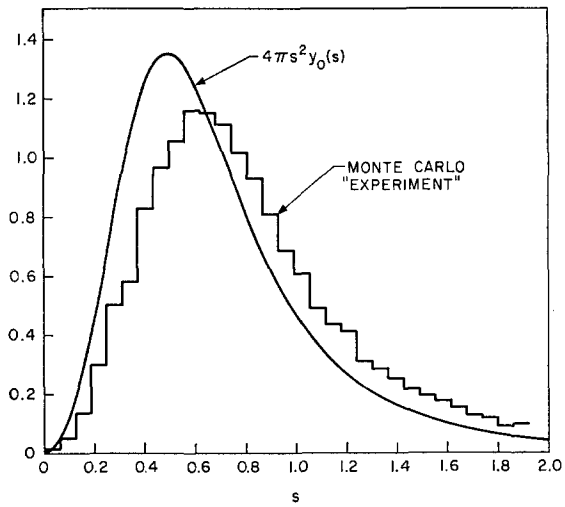

FIG. 3. Comparison of analytic approximation $4\pi s^2 y_0(s)$ and the Monte Carlo "experimental" result for ideal-gas pair size distribution. The unit cube used for the Monte Carlo determination has edge length equal to about 8.5 times the distance corresponding to the histogram peak.

One is forced to the conclusion that $y(s)$ decays to zero more slowly than an exponential function. The obvious alternative is an inverse power law for a large-s tail,

$$y(s)\sim(l/s)^n. \tag{12}$$

In order to replicate an inverse power upon inserting the function $y(sx)$ in the exponential right-hand member of Eq. (9), the integral term must vary logarithmically with s in this large-s regime.

The plausibility of algebraic decay form (12) may be supported if we permit a small modification of the function $h(x)$ defined in Eq. (6). Let

$$\begin{aligned} h_0(x) &= x^3 \qquad (0\leq x\leq 1) \\ &= 1 \qquad (1\leq x<\infty); \end{aligned} \tag{13}$$

this modified function also satisfies functional relation (7), and is shown by Fig. 2 to differ from $h(x)$ in $\frac{1}{3}<x<3$ only by a slight amount. The h_0 analog of the nonlinear integral equation (9),

$$y_0(s) = \exp\left[-\left(\frac{32\pi^2}{3}\right)s^6\int_0^\infty x^2 h_0(x)\,y_0(sx)\,dx\right], \tag{14}$$

is easily seen to have the solution

$$y_0(s) = [1+(4\pi/3)s^3]^{-2}. \tag{15}$$

Under the presumption that replacement of h by h_0 causes little change, we tentatively identify l and n in Eq. (12) thus:

$$\begin{aligned} l &= (3/4\pi)^{1/3}, \\ n &= 6. \end{aligned} \tag{16}$$

It is perhaps significant to note that $y_0(s)$ *exactly* satisfies normalization condition (10).

To provide an independent test of the approximate size distribution $4\pi s^2 y_0(s)$ just obtained, a Monte Carlo "experiment" was also carried out by electronic computer. One hundred fifty points each of $-$ and $+$ designation were generated at random within a cube, and the requisite pairing carried out under periodic boundary conditions. The composite result of 100 such runs is presented in histogram form in Fig. 3, along with the analytic result $4\pi s^2 y_0(s)$. As judged by this Monte Carlo result, one concludes that the primary error in the binary-cluster approximation is that the distance scale is compressed, for the maximum in $4\pi s^2 y_0(s)$ occurs only at about 80% of the correct s value. Nevertheless the binary-cluster approach does seem to retain the correct qualitative sense of the pairing process.

With regard to the postulated algebraic tail, the statistics of the computer experiment do not provide definitive characterization. On the required log–log plot, however, our sparse results at large s are definitely *not* consistent with an exponential decay, but *are* consistent with power law (12) with n approximately 6.

A final piece of evidence favoring the power law (12) with $n=6$, in the form of another nonlinear integral equation that must be satisfied by the size distribution $p^{(1)}(s)$, is derived and analyzed in Appendix A.

III. PAIRING OF IDENTICAL RIGID SPHERES

The next case to examine is that of equal numbers of geometrically identical uncharged rigid spheres, indexed $-$ and $+$. They will again be paired by the previous rules.

The most obvious modification of size distribution $p^{(1)}(s_1)$ caused by the sphere collision diameter a is that this function now must vanish identically for $s_1<a$. In

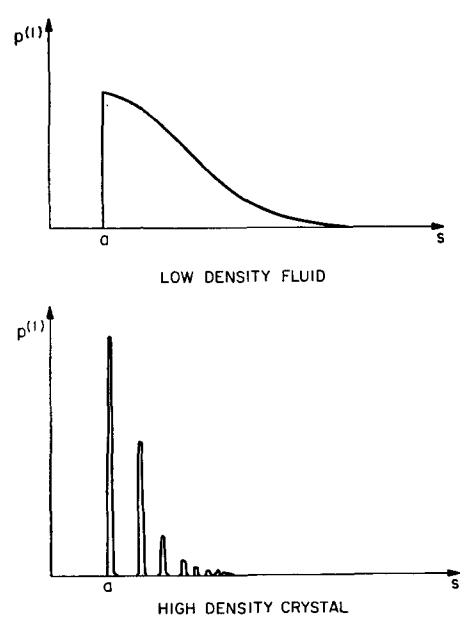

FIG. 4. Qualitative character of particle-pair size distributions for rigid spheres at low and high density.

the event that the rigid spheres form a dilute fluid, however, their distribution outside a given sphere at distances greater than a should be essentially identical to the ideal-gas distribution. For this reason, we expect $p^{(1)}(s_1)$ in the dilute rigid-sphere limit to be merely a cutoff version (for $s_1<a$) of the ideal-gas function, suitably renormalized.

If the rigid spheres are densely packed, however, $p^{(1)}(s_1)$ must exhibit marked deviations from the ideal-gas form, resulting from the formation of a crystalline phase. Although the − and + particles will be randomly distributed throughout the crystal, in the close-packed limit only discrete pair distances will occur corresponding to the well-defined coordination shells. Likewise $p^{(1)}(s_1)$ can be nonzero only at these discrete distances, and must vanish between. At slightly less than the close-packed density the existence of coordination shells will still produce many peaks in $p^{(1)}(s_1)$, as shown schematically in Fig. 4.

Whether or not a dense fluid of rigid spheres would also exhibit several $p^{(1)}(s_1)$ maxima (reflecting rudimentary short-range crystalline order) can be answered only by detailed computation. We shall not attempt such a computation here in part because of its difficulty, but also because we do not require the results for the electrolyte calculation performed below.

So far as qualitative understanding of rigid-sphere pairing in this intermediate density range is concerned, it is instructive to recall the character of the conventional rigid-sphere pair correlation function.[7] Though the most accurate evaluations of this quantity produce damped oscillations indicative of local quasicrystalline order,[8] the fact remains that spheres at large distance in the fluid are totally uncorrelated, exactly as is the case for ideal gases. At an intermediate stage of the particle-pairing process when a given + sphere, say, is looking for a − partner at these distances large compared to a, the pairing process should proceed exactly as it does in the ideal-gas mixture. One must therefore conclude that the hard sphere $p^{(1)}(s_1)$ also has an inverse sixth-power tail.[9]

We can easily specify the beginnings of a development of $p^{(1)}(s_1)$ in powers of (s_1-a). Let $g^{(2)}$ and $g^{(3)}$, respectively, stand for the rigid-sphere pair and triplet correlation functions (they reduce to unity for separated particles). Consider a spherical shell of thickness ds_1 and radius s_1 just slightly larger than collision diameter a for a centrally located + sphere, as shown in Fig. 5. The chance of finding some − sphere in this shell is $[(N/V)g^{(2)}(s_1)]4\pi s_1^2 ds_1$. If this close-by − exists, it will be paired with the central + *unless*:

(a) the central + has already been paired with an even closer −;

(b) the spherical-shell − has been paired with some other + at distance less than s_1 from it;

(c) both the central + and spherical-shell − have other partners.

By comparison with events (a) and (b), the last of these three possibilities leads to higher-order corrections which we neglect. The remaining possibilities are predicated upon the simultaneous occurrence of a triplet of spheres, and will thus naturally bring in $g^{(3)}$.

The geometry of cases (a) and (b) is a fact identical, so twice the same $g^{(3)}$ integral must be subtracted in the result,

$$(4\pi s_1^2 ds_1)\left(\frac{N}{V}\right)^{-1} p^{(1)}(s_1) \cong \left(\frac{N}{V}\right) g^{(2)}(s_1)(4\pi s_1^2 ds_1) \times \left[1-2\left(\frac{N}{V}\right)\int_a^{s_1} s_2^2 ds_2 \int_0^{2\pi} d\phi_2 \int_0^{\pi} \sin\theta_{12} d\theta_{12} \frac{g^{(3)}(s_1, s_2, \theta_{12})}{g^{(2)}(s_1)}\right]. \quad (17)$$

The distance variables s_1, s_2, and angle θ_{12} locate the two other spheres in the neighborhood of the central particle. In view of the smallness of (s_1-a) and (s_2-a), however, we may take in leading order

$$g^{(3)}(s_1, s_2, \theta_{12})/g^{(2)}(s_1) \cong g^{(3)}(a, a, \theta_{12})/g^{(2)}(a) \quad (18)$$

in Eq. (17). Therefore one obtains the following result,

$$p^{(1)}(s_1) = \left(\frac{N}{V}\right) g^{(2)}(a) + \left[\left(\frac{N}{V}\right)\left(\frac{\partial g^{(2)}(r)}{\partial r}\right)_{r=a} - 4\pi\left(\frac{Na}{V}\right)^2 \int_{\pi/3}^{\pi} g^{(3)}(a, a, \theta_{12}) \sin\theta_{12} d\theta_{12}\right](s_1-a) + O[(s_1-a)^2]. \quad (19)$$

The lower integration limit in this last expression results from sphere impenetrability; it is the smallest angle possible between the direction to the centers of two spheres from the center of a third sphere on which they are rolling.

It seems clear that asymptotic development (19) could in principal be extended to higher order in (s_1-a). The results would inevitably involve higher and higher-order rigid-sphere $g^{(n)}$'s, since simultaneous occurrences involving ascending numbers of particles at small distances must be taken into account. Since so

[7] J. G. Kirkwood, E. K. Maun, and B. J. Alder, J. Chem. Phys. **18**, 1040 (1950).

[8] G. J. Throop and R. J. Bearman, J. Chem. Phys. **42**, 2408 (1965).

[9] Owing to modifications at small s_1 in $p^{(1)}(s_1)$, and the requirement of normalization, the multiplicative constant for this tail will differ from the ideal-gas value.

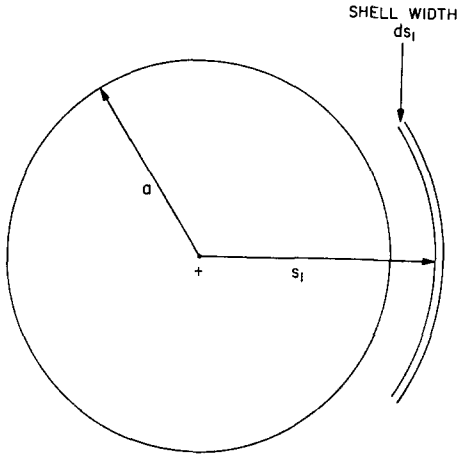

FIG. 5. Differential spherical shell, concentric with a fixed + particle, used in estimating $p^{(1)}(s_1)$ for small (s_1-a).

little quantitative information is available about these functions, the utility of succeeding terms beyond the ones explicitly given in Eq. (19) is minimal.

Eventually it will be profitable to carry out rigid-sphere Monte Carlo computer experiments to obtain $p^{(1)}(s_1)$ at various densities. If they were done in sufficient accuracy, it should be possible to test our conclusion about the persistence of a sixth-power tail.

IV. EXTERNAL FIELD RENORMALIZATION

The next aspect of the development working toward consideration of the actual electrolyte concerns a computational shortcut. Since we shall have to examine the way in which the pairs of particles as "dipolar molecules" orient statistically under an applied torque, due attention must be given the steric hindrance potential $u(\mathbf{x}_1, \mathbf{x}_2)$, and its effect upon such orientation. For the types of statistical averages that are relevant ultimately to calculation of the electrolyte dielectric response it is fortunate that the effect of the hindrances may be simply relegated to a renormalization constant.

We shall continue to focus attention on the mixture of geometrically identical rigid spheres, comprising equal numbers of − and + particles. Let there be applied to the initially homogeneous fluid mixture a sinusoidal external field, which adds to the Hamiltonian a sum of single-particle potential energies,

$$U_0\left[-\sum_{i=1}^{N}\sin(\mathbf{k}\cdot\mathbf{r}_i)+\sum_{i=N+1}^{2N}\sin(\mathbf{k}\cdot\mathbf{r}_i)\right], \quad (20)$$

where U_0 is a coupling strength parameter, and the − particles are numbered 1 to N, the + particles $N+1$ to $2N$. If U_0 is sufficiently weak, it produces only a linear response in the hard-sphere mixture whereby a small degree of local unmixing occurs (though to the same linear order the total sphere density remains unchanged). One may easily calculate the difference in singlet densities produced by potential (20) using the standard technique of functional differentiation of the partition function[10];

$$\rho_+^{(1)}(\mathbf{r})-\rho_-^{(1)}(\mathbf{r})=-(2\beta U_0 N/V)\sin(\mathbf{k}\cdot\mathbf{r})+O(U_0^3). \quad (21)$$

Normally such linear response to an external potential requires knowledge of the system's pair correlation functions, but the especially simple result (21) reflects the model symmetry with respect to + and − particles.

Next we shall focus attention on a single +, − pair produced by the previously advocated pairing scheme. In particular we inquire into the effect of the same type of sinusoidal potential as shown in Eq. (20), but with a different strength U_0'. When the pair has configuration $\mathbf{x}=\mathbf{R}\oplus\mathbf{s}$, it will experience a torque potential

$$U(\mathbf{x})=U_0'\{\sin[\mathbf{k}\cdot(\mathbf{R}+\tfrac{1}{2}\mathbf{s})]-\sin[\mathbf{k}\cdot(\mathbf{R}-\tfrac{1}{2}\mathbf{s})]\}$$
$$=2U_0'\cos(\mathbf{k}\cdot\mathbf{R})\sin(\tfrac{1}{2}\mathbf{k}\cdot\mathbf{s}). \quad (22)$$

This torque potential will surely perturb the size distribution $p^{(1)}$ of the pairs, rendering this function dependent upon both orientation and center position. We may write the following expression for the perturbed distribution:

$$p^{(1)}(s)+\delta p^{(1)}(\mathbf{R},\mathbf{s}), \quad (23)$$

where the first term is the isotropic unperturbed size distribution, and $\delta p^{(1)}$ is the change induced by $U(\mathbf{x})$.

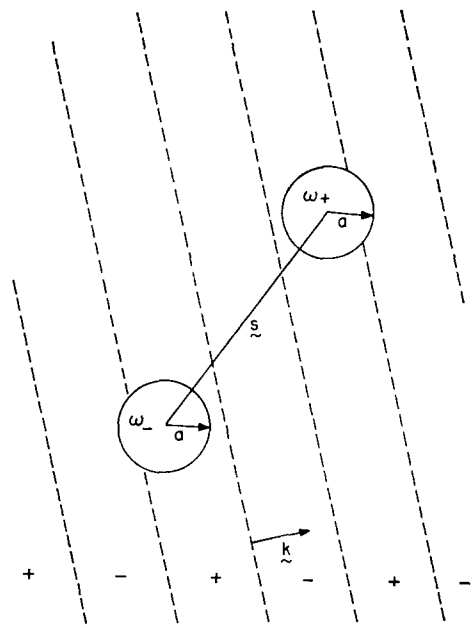

FIG. 6. Charge density induced by ψ_{ap} in the vicinity of a fixed ion pair with separation $\mathbf{s}$. The wave vector $\mathbf{k}$ determines the spatial variation of ψ_{ap}. It is assumed that the only local effect of the fixed pair is exclusion of charge from the spheres ω_- and ω_+ of radius a surrounding its ends. The parallel dotted lines are nodes of $\rho_{in}(\mathbf{r})$.

[10] J. L. Lebowitz and J. K. Percus, J. Math. Phys. 4, 116 (1963).

Obviously $\delta p^{(1)}$ alone will contribute to a singlet density difference of the type shown in Eq. (21). In the event that one could disregard hindrances between different particle pairs, a very simple expression for $\delta p^{(1)}$ is available, since the perturbed distribution may be obtained merely by multiplying $p^{(1)}(s)$ by a Boltzmann factor containing $U(\mathbf{x})$,[11]

$$p^{(1)}(s)+\delta p^{(1)}(\mathbf{R},\mathbf{s})=p^{(1)}(s)\exp[-\beta U(\mathbf{x})];$$
$$\delta p^{(1)}(\mathbf{R},\mathbf{s})=-\beta U(\mathbf{x})p^{(1)}(s), \quad (24)$$

to order $(U_0')^2$. The implied singlet density difference may next be found by integrating out the internal variable $\mathbf{s}$ for pairs in favorable positions to contribute to the spatial position $\mathbf{r}$ of interest,

$$\rho_+^{(1)}(\mathbf{r})-\rho_-^{(1)}(\mathbf{r})$$
$$=\int d\mathbf{s}[\delta p^{(1)}(\mathbf{r}-\tfrac{1}{2}\mathbf{s},\mathbf{s})-\delta p^{(1)}(\mathbf{r}+\tfrac{1}{2}\mathbf{s},\mathbf{s})]. \quad (25)$$

By using Eqs. (22) and (24), we may convert this last expression to the following one:

$$\rho_+^{(1)}(\mathbf{r})-\rho_-^{(1)}(\mathbf{r})=-\frac{2\beta U_0' N}{V}\sin(\mathbf{k}\cdot\mathbf{r})$$
$$\times\int ds\left(\frac{N}{V}\right)^{-1}p^{(1)}(s)[1-\cos(\mathbf{k}\cdot\mathbf{s})]. \quad (26)$$

The reason that the two expressions shown in Eqs. (21) and (26) for $\rho_+^{(1)}-\rho_-^{(1)}$ do not agree when $U_0'=U_0$ is precisely due to neglect of steric hindrance between pairs. They would formally agree if

$$U_0'/U_0=\lambda(k),$$
$$\lambda(k)=\left[4\pi\int_0^\infty s^2\left(1-\frac{\sin(ks)}{ks}\right)\left(\frac{N}{V}\right)^{-1}p^{(1)}(s)\,ds\right]^{-1}. \quad (27)$$

For small k, $\sin(ks)/ks$ in the integral will be close to unity over most of the integration range for which $p^{(1)}(s)$ is significant, so consequently $\lambda(k)$ is very large. On the other hand $\lambda(k)$ will just become unity as $k\to\infty$, since the rapid oscillations of the trigonometric factor are inconsequential, and thus leave merely the size-distribution normalization integral,

$$4\pi\left(\frac{N}{V}\right)^{-1}\int_0^\infty s^2 p^{(1)}(s)\,ds=1. \quad (28)$$

These features of $\lambda(k)$ are fully consistent with the character of pair steric hindrance previously established. Because the hindrance potential $u(\mathbf{x}_i,\mathbf{x}_j)$ acts repulsively between opposite ends of pairs (as shown for example by Fig. 1), there will be a statistical tendency for neighboring pairs of average size to line up parallel to one another to minimize u's effect. As one such pair reorients under the influence of a torque potential such as $U(\mathbf{x})$ in Eq. (22), when k is not too large, it will tend to "drag" its neighbor pairs along, thus giving them an extra reorienting agency. On the other hand when k is so large that $U(\mathbf{x})$ possesses many oscillations over an average pair length, any one pair of given size can experience many different directions of potential minimum; the net effect of "drag" by incoherently orienting neighbors on a given pair obviously will be small.

We shall proceed to the central electrolyte dielectric response calculation in the next section under the assumption that $\lambda(k)$ may be treated as a renormalization constant whose use embodies adequate treatment of steric hindrance. Thus, whenever a torque potential of strength U_0 acts on the particle pairs in the system, we shall replace the strength simply by $U_0\lambda(k)$, and proceed as though the pairs did not interfere with one another through short-range forces resulting either from their rigid-sphere potentials or from $u(\mathbf{x})$. By way of justifying this shortcut, it should be stressed that $\lambda(k)$ in Eq. (27), regarded as a functional of $p^{(1)}$, is more general than indicated merely by our present hard-sphere context, since exactly the same form results from any assumed short-range force acting between all particles in the system.

V. APPROXIMATE ELECTROLYTE DIELECTRIC RESPONSE

Finally we consider the primitive electrolyte model, for which those rigid spheres indexed $-$ bear charge $-Ze$, and those indexed $+$ bear charge $+Ze$. Our task is evaluation of the electrolyte dielectric response function $\epsilon(k)$.

In Sec. III of Paper I it was stated that if an external electrostatic potential

$$\psi_{ap}(\mathbf{r})=(\psi_0/\epsilon_0)\sin(\mathbf{k}\cdot\mathbf{r}) \quad (29)$$

was applied to the system (ϵ_0 is the solvent dielectric constant), the ions would rearrange so as to shield this potential. The resulting average potential $\bar{\Psi}$ would then define $\epsilon(k)$,

$$\bar{\Psi}(\mathbf{r})=[\psi_0/\epsilon(k)]\sin(\mathbf{k}\cdot\mathbf{r}), \quad (30)$$

and the induced ionic charge density performing the shielding would be

$$\rho_{in}(\mathbf{r})=(\psi_0 k^2/4\pi)\{[\epsilon_0/\epsilon(k)]-1\}\sin(\mathbf{k}\cdot\mathbf{r}). \quad (31)$$

The mean potential $\bar{\Psi}$ will form the basis for a torque calculation on a given ion pair, exactly as done in the preceding section, and for which the renormalization factor $\lambda(k)$ is appropriate.

Even in the electrolyte undisturbed by ψ_{ap} we know that there is an average charge density that accumulates

[11] To the linear order in U_0' in which we work, normalization of the size distribution is preserved.

around any given ion pair as a result of the action of the steric-hindrance potential $u(\mathbf{x}_i, \mathbf{x}_j)$. However this charge must have axial symmetry with respect to the pair around which it accumulates, so although it moves around as the pair moves, it cannot exert any mean torque on that pair.

Instead, we must be concerned only with the extra charge density that builds up around a given fixed pair under the influence of ψ_{ap}. Of course no such charge can occur inside the two spherical exclusion volumes ω_- and ω_+ with radius a surrounding the ends of the fixed pair; far from the pair, however the charge density should agree precisely with $\rho_{in}(\mathbf{r})$ in Eq. (31). The central assumption to be used is that the functional form $\rho_{in}(\mathbf{r})$ applies everywhere outside the radius-a spherical surfaces for the pair's ends. Figure 6 provides an illustration for this assumption.

Were it not for the induced charge excluded from the two spherical regions, $\bar{\Psi}(\mathbf{r})$ itself would be the correct potential to use in a mean torque calculation. However we must employ in its place a modified mean electrostatic potential $\psi^*(\mathbf{r};\mathbf{s})$; this is the potential at position $\mathbf{r}$ which is at the center of a radius-a exclusion sphere, while another radius-a exclusion sphere also lies at position $\mathbf{r}+\mathbf{s}$. In terms of Fig. 6, $\psi^*(\mathbf{r};\mathbf{s})$ will be the mean electrostatic potential (exclusive of the fixed-pair self-potential) at the center of the $-$ end exclusion sphere. The corresponding perturbed singlet ion-pair distribution function involves a Boltzmann factor with the product of ψ^* and renormalization factor $\lambda(k)$,

$$p^{(1)}(s)+\delta p^{(1)}(\mathbf{R},\mathbf{s})=p^{(1)}(s)\,\exp\{-\beta Ze\lambda(k)[\psi^*(\mathbf{R}+\tfrac{1}{2}\mathbf{s};-\mathbf{s})-\psi^*(\mathbf{R}-\tfrac{1}{2}\mathbf{s};\mathbf{s})]\}; \tag{32}$$

only the linear approximation is relevant, so

$$\delta p^{(1)}(\mathbf{R},\mathbf{s})=\beta Ze\lambda(k)\,p^{(1)}(s)[\psi^*(\mathbf{R}-\tfrac{1}{2}\mathbf{s};\mathbf{s})-\psi^*(\mathbf{R}+\tfrac{1}{2}\mathbf{s};-\mathbf{s})]. \tag{33}$$

The induced charge density, whose phenomenological form has already been given in Eq. (31), may next be expressed in terms of $\delta p^{(1)}$, exactly as was done for uncharged rigid spheres in the previous section, Eq. (25):

$$\rho_{in}(\mathbf{r})=Ze\int d\mathbf{s}[\delta p^{(1)}(\mathbf{r}-\tfrac{1}{2}\mathbf{s},\mathbf{s})-\delta p^{(1)}(\mathbf{r}+\tfrac{1}{2}\mathbf{s},\mathbf{s})]. \tag{34}$$

By utilizing Eq. (33) for $\delta p^{(1)}$, we find

$$\rho_{in}(\mathbf{r})=2\beta(Ze)^2\lambda(k)\int d\mathbf{s}p^{(1)}(s)[\psi^*(\mathbf{r}+\mathbf{s};-\mathbf{s})-\psi^*(\mathbf{r};\mathbf{s})]. \tag{35}$$

The potential $\psi^*(\mathbf{r};\mathbf{s})$ may be regarded as consisting of three parts. The first is just $\bar{\Psi}(\mathbf{r})$ itself, Eq. (30). The second arises from the missing charge that would otherwise have occupied ω_-, the radius-a sphere surrounding position $\mathbf{r}$. The third is the potential change due to the remaining missing charge in the other exclusion sphere ω_+; since ω_+ and ω_- overlap to some extent when $s<2a$, this last charge should be reckoned only on the basis of the region

$$\omega^*(\mathbf{r},\mathbf{s})=\omega_+(\mathbf{r}+\mathbf{s})-\omega_+(\mathbf{r}+\mathbf{s})\cap\omega_-(\mathbf{r}) \tag{36}$$

in the standard set-theoretic notation. Thus

$$\psi^*(\mathbf{r};\mathbf{s})=\bar{\Psi}(\mathbf{r})-\int_{\omega_-(\mathbf{r})}\frac{\rho_{in}(\mathbf{r}')}{\epsilon_0|\mathbf{r}-\mathbf{r}'|}\,d\mathbf{r}'-\int_{\omega^*(\mathbf{r},\mathbf{s})}\frac{\rho_{in}(\mathbf{r}')}{\epsilon_0|\mathbf{r}-\mathbf{r}'|}\,d\mathbf{r}'. \tag{37}$$

Owing to the simple shape of $\omega_-(\mathbf{r})$, the first of these integrals is easy to perform, so

$$\psi^*(\mathbf{r};\mathbf{s})=\psi_0\sin(\mathbf{k}\cdot\mathbf{r})\,([\epsilon(k)]^{-1}+\{\epsilon_0^{-1}-[\epsilon(k)]^{-1}\}[1-\cos(ka)])-\int_{\omega^*(\mathbf{r},\mathbf{s})}\frac{\rho_{in}(\mathbf{r}')}{\epsilon_0|\mathbf{r}-\mathbf{r}'|}\,d\mathbf{r}'. \tag{38}$$

Substitution of this last expression for ψ^* into Eq. (35) yields the following implicit relation for the induced charge density:

$$\rho_{in}(\mathbf{r})=2\beta(Ze)^2\psi_0\frac{N}{V}\,(-[\epsilon(k)]^{-1}+\{[\epsilon(k)]^{-1}-\epsilon_0^{-1}\}[1-\cos(ka)])\sin(\mathbf{k}\cdot\mathbf{r})$$
$$+\frac{2\beta(Ze)^2\lambda(k)}{\epsilon_0}\int d\mathbf{s}p^{(1)}(s)\left[\int_{\omega^*(\mathbf{r},\mathbf{s})}d\mathbf{r}'\,\frac{\rho_{in}(\mathbf{r}')}{|\mathbf{r}-\mathbf{r}'|}-\int_{\omega^*(\mathbf{r}+\mathbf{s},-\mathbf{s})}d\mathbf{r}'\,\frac{\rho_{in}(\mathbf{r}')}{|\mathbf{r}+\mathbf{s}-\mathbf{r}'|}\right]. \tag{39}$$

The phenomenological ρ_{in} form in Eq. (31) may be utilized now to eliminate this quantity from under the integrals in Eq. (39). In doing so, it proves convenient to employ the formally exact device of averaging both

occurrences of $\rho_{in}(\mathbf{r}')$ over the $|\mathbf{r}-\mathbf{r}'|=$const sphere. One ultimately finds that Eq. (39) is transformed to

$$\rho_{in}(\mathbf{r})=2\beta(Ze)^2\psi_0\frac{N}{V}\sin(\mathbf{k}\cdot\mathbf{r})\Big[-[\epsilon(k)]^{-1}+\{[\epsilon(k)]^{-1}-\epsilon_0^{-1}\}[1-\cos(ka)]$$
$$+\frac{k\lambda(k)}{4\pi}\{[\epsilon(k)]^{-1}-\epsilon_0^{-1}\}\int d\mathbf{s}\left(\frac{N}{V}\right)^{-1}p^{(1)}(s)[I_1(s,k)-I_2(s,k)]\Big], \quad (40)$$

where

$$I_1(s,k)=\int_{\omega*(\mathbf{r},\mathbf{s})}d\mathbf{r}'\,\frac{\sin(k|\mathbf{r}-\mathbf{r}'|)}{|\mathbf{r}-\mathbf{r}'|^2},$$
$$I_2(s,k)=\int_{\omega*(\mathbf{r}+\mathbf{s},-\mathbf{s})}d\mathbf{r}'\,\frac{\sin(k|\mathbf{r}-\mathbf{r}'|)}{|\mathbf{r}-\mathbf{r}'||\mathbf{r}+\mathbf{s}-\mathbf{r}'|}. \quad (41)$$

Bipolar coordinates[12] are useful in transforming each of I_1 and I_2 to definite single integrals for all $s\geq a$:

$$I_1(s,k)=\frac{\pi}{s}\int_{\max(a,s-a)}^{s+a}[a^2-(s-t)^2]\frac{\sin(kt)\,dt}{t},$$
$$I_2(s,k)=\frac{2\pi}{s}\int_0^a[s+t-\max(a,|s-t|)]\sin(kt)\,dt. \quad (42)$$

The first of these may be expressed in terms of the integral sine function

$$\mathrm{Si}(x)=\int_0^x\frac{\sin(t)\,dt}{t}=x-\frac{x^3}{3\cdot3!}+\frac{x^5}{5\cdot5!}-\frac{x^7}{7\cdot7!}+\cdots,\qquad \mathrm{Si}(+\infty)=\tfrac{1}{2}\pi, \quad (43)$$

with the result

$$I_1(s,k)=\frac{\pi}{s}\Big((a^2-s^2)\{\mathrm{Si}[k(s+a)]-\mathrm{Si}(ka)\}+\frac{2s-a}{k}\cos(ka)+\frac{a-s}{k}\cos[k(s+a)]$$
$$+\frac{1}{k^2}\{\sin(ka)-\sin[k(s+a)]\}\Big)\qquad (a\leq s\leq 2a),$$
$$=\frac{\pi}{s}\Big((a^2-s^2)\{\mathrm{Si}[k(s+a)]-\mathrm{Si}[k(s-a)]\}+\frac{s+a}{k}\cos[k(s-a)]$$
$$+\frac{a-s}{k}\cos[k(s+a)]-\frac{2}{k^2}\sin(ka)\cos(ks)\Big)\qquad (2a\leq s). \quad (44)$$

The quantity I_2 on the other hand is elementary,

$$I_2(s,k)=(2\pi/k^2s)\{\sin(ka)-ks\cos(ka)+\sin[k(s-a)]\}\qquad (a\leq s\leq 2a),$$
$$=(4\pi/k^2s)[\sin(ka)-ka\cos(ka)]\qquad (2a\leq s). \quad (45)$$

Let

$$\tau(k)=\left(\frac{N}{V}\right)^{-1}\int_0^\infty s^2p^{(1)}(s)[I_1(s,k)-I_2(s,k)]ds; \quad (46)$$

Eq. (40) then is equivalent to

$$\rho_{in}(\mathbf{r})=2\beta(Ze)^2\psi_0(N/V)\sin(\mathbf{k}\cdot\mathbf{r})\,(-[\epsilon(k)]^{-1}$$
$$+\{[\epsilon(k)]^{-1}-\epsilon_0^{-1}\}[1-\cos(ka)+k\lambda(k)\tau(k)]). \quad (47)$$

The condition that this formula agree with the phenomenological equation (31) for $\rho_{in}(\mathbf{r})$ constitutes a determining algebraic equation for the electrolyte's dielectric response function $\epsilon(k)$. The solution is

$$\frac{\epsilon_0}{\epsilon(k)}=1-\frac{\kappa^2}{k^2+\kappa^2[\cos(ka)-k\lambda(k)\tau(k)]},$$
$$\kappa^2=8\pi N(Ze)^2/\epsilon_0k_BTV. \quad (48)$$

[12] T. L. Hill, *Statistical Mechanics* (McGraw-Hill Book Co., New York, 1956), p. 203.

VI. ELECTROLYTE FREE ENERGY

The ion-atmosphere charge density for the primitive-electrolyte model is described by the difference between the two independent ionic-doublet correlation functions, $g_{++}^{(2)}(r)-g_{+-}^{(2)}(r)$. It was shown in Eq. (47) of Paper I that the correct dielectric function $\epsilon(k)$ for the electrolyte gives exactly this difference as an integral transform,

$$Ze\frac{N}{V}[g_{++}^{(2)}(r)-g_{+-}^{(2)}(r)]=-\frac{Ze}{2\pi^2 r}\times\int_0^\infty k\sin(kr)\left\{\frac{k^2}{\kappa^2}\left[\frac{\epsilon_0}{\epsilon(k)}-1\right]+1\right\}dk. \quad (49)$$

It is our purpose now to pursue the implications of the specific $\epsilon(k)$ result just obtained in Eq. (48).

In the event that hard-core diameter a were negligible, $\tau(k)$ defined in Eq. (46) would vanish, and Eq. (48) would reduce to an elementary expression to be identified with the linear Debye–Hückel point-ion theory,

$$\epsilon_0/\epsilon(k)\cong 1-[\kappa^2/(k^2+\kappa^2)]. \quad (50)$$

Indeed, insertion of this expression into Eq. (49) produces the well-known result

$$Ze(N/V)[g_{++}^{(2)}(r)-g_{+-}^{(2)}(r)]\cong-[Ze\kappa^2\exp(-\kappa r)/4\pi r]. \quad (51)$$

The quantity $\tau(k)$ represents a cross interaction between the two exclusion spheres ω_+ and ω_- in Fig. 6. At low electrolyte concentration the mean distance between these spheres will be large, so interaction quantity τ will be negligible even without assuming a is negligible. In this case the denominator in our dielectric response function reduces to $k^2+\kappa^2\cos(ka)$. This particular denominator combination has been produced several times before in statistical-mechanical theories of electrolytes,[2–4,13] though not previously identified as a dielectric response. The correction term $-\kappa^2 k\lambda(k)\tau(k)$ that arises in the present theory surely must become important at intermediate and high concentration.

On account of the ions' rigid cores, the integral transform (49) must vanish identically for all $0\leq r<a$. The approximate $\epsilon(k)$ result (48) no doubt is somewhat imprecise, and could not *a priori* be expected to satisfy this identity. However, we shall presume to use Eq. (48) only for $r>a$.

Since $\epsilon(k)$ is an even function of k, the integral in Eq. (49) may be extended along the entire real axis,

$$\frac{ZeN}{V}[g_{++}^{(2)}(r)-g_{+-}^{(2)}(r)]=-\frac{Ze}{4\pi^2 ir}\int_{-\infty}^{+\infty}k\exp(ikr)\left\{\frac{k^2}{\kappa^2}\left[\frac{\epsilon_0}{\epsilon(k)}-1\right]+1\right\}dk. \quad (52)$$

This form is especially suited to evaluation by the method of residues, and we employ that procedure first on the integral resulting from neglect of the $-\kappa^2 k\lambda(k)\tau(k)$ correction:

$$\frac{ZeN}{V}[g_{++}^{(2)}(r)-g_{+-}^{(2)}(r)]\cong-\frac{Ze\kappa^2}{4\pi^2 ir}\int_{-\infty}^{+\infty}\frac{k\exp(ikr)\cos ka}{k^2+\kappa^2\cos(ka)}dk. \quad (53)$$

When $r>a$ the contour may be closed along the infinite semicircle in the upper half-plane, with the eventual result

$$\frac{ZeN}{V}[g_{++}^{(2)}(r)-g_{+-}^{(2)}(r)]\cong-\frac{Ze\kappa^2}{2\pi r}\sum_{j=1}^{\infty}A_j\exp(ik_j r),$$
$$A_j=k_j\cos(k_j a)/[2k_j-\kappa^2 a\sin(k_j a)]. \quad (54)$$

The summation covers all roots k_j of the transcendental equation

$$k^2+\kappa^2\cos(ka)=0 \quad (55)$$

enclosed by the integration contour.

Appendix B provides a detailed analysis of the k_j which are in fact infinite in number. In the small-κ limit it is found that all k_j but one have diverging (positive) imaginary parts, and the corresponding rapidly damped exponentials in Eq. (54) are negligible. The single exception may be taken as k_1, for which one finds

$$k_1\sim i\kappa. \quad (56)$$

The single surviving term is in precise agreement with the familiar Debye–Hückel result (51) for $r>a$. The terms with $j>1$ in Eq. (54) presumably provide an approximate account of local ion order at distances comparable with a in the moderate-to-high κ regime.

The incorporation of our correction term $-\kappa^2 k\lambda(k)\tau(k)$ in $\epsilon(k)$ forces consideration of a shifted set of roots k_j' of the new transcendental equation

$$k^2+\kappa^2[\cos(ka)-k\lambda(k)\tau(k)]=0. \quad (57)$$

Owing to the universality of the Debye–Hückel limiting law as $\kappa\to 0$, we expect again to find in the upper-half

[13] J. G. Kirkwood, Chem. Rev. **19**, 275 (1936).

complex-k plane a root k_1' asymptotic to $i\kappa$. Therefore to establish the lowest-order effect of the correction term on this root, it suffices to utilize the small-κ limit for this correction. From Eqs. (27) and (43)–(46) we find for small k

$$k\lambda(k)\tau(k)\sim T_0k^2,$$

$$T_0=\left[\int_a^\infty s^4p^{(1)}(s)\,ds\right]^{-1}\times\left[\int_a^{2a}\left[-\tfrac{1}{60}s^6+\tfrac{1}{8}(as^5)-\tfrac{1}{3}(a^2s^4)\right]p^{(1)}(s)\,ds+\int_{2a}^\infty\left[-\tfrac{1}{3}(a^3s^3)+\tfrac{1}{15}(2a^5s)\right]p^{(1)}(s)\,ds\right]. \quad (58)$$

The net result of incorporating this result into the $\epsilon(k)$ expression (48) is the following:

$$\epsilon_0/\epsilon(k)\cong 1-\{\kappa^2/[(1-T_0\kappa^2)k^2+\kappa^2\cos(ka)]\}. \quad (59)$$

Formal substitution of this last expression into the general ion-atmosphere formula (52) produces an expression which may be compared with the corresponding "uncorrected" version in Eq. (53),

$$\frac{ZeN}{V}[g_{+\,+}^{(2)}(r)-g_{+\,-}^{(2)}(r)]=-\frac{Ze\kappa^2}{4\pi^2ir}\int_{-\infty}^{+\infty}\frac{k\exp(ikr)[\cos(ka)-T_0k^2]}{(1-T_0\kappa^2)k^2+\kappa^2\cos(ka)}\,dk. \quad (60)$$

Once again the method of residues can be used to evaluate the last integral, and will generate a sum of exponentials as before. Because Eq. (60) has relied upon the small-k expression (59), we can only expect accuracy for the least rapidly decaying exponential, the one corresponding to root k_1'. Even with retention of the full functional form for the correction term, though, it is no doubt true that our $\epsilon(k)$ calculation has least error for small k. The fact is that we were forced to make specific assumptions in the previous section about local ordering of ion pairs under the influence of external fields, and the imprecision of the assumptions should be most evident for large k (wavelengths comparable to the range of that order). Therefore we shall use the explicit form (60) *only* to determine the least rapidly decaying component of the ion atmosphere, and the remainder of shorter range will be subject to independent determination.

Thus Eq. (60) leads us to write

$$\frac{4\pi N}{V}[g_{+\,+}^{(2)}(r)-g_{+\,-}^{(2)}(r)]=\frac{(k_1')^2\exp(ik_1'r)}{[1-T_0\kappa^2-(\kappa^2a/2k_1')\sin(k_1'a)]r}+\frac{f(r)}{r}. \quad (61)$$

As before, the precise multiplicative factor for the principal ion-atmosphere decay term has been assigned by the appropriate residue in Eq. (60). The function $f(r)$ then comprises the totality of the shorter-ranged contributions. The root k_1' satisfies

$$(k_1')^2+[\kappa^2/(1-T_0\kappa^2)]\cos(k_1'a)=0, \quad (62)$$

which is the same as the preceding transcendental equation (55), except for inclusion of an "effective κ^2." We may therefore use Eq. (B5) of Appendix B to achieve a low-κ development of $(k_1')^2$,

$$(k_1')^2=-\kappa^2\{1+(\tfrac{1}{2}a^2+T_0)\kappa^2+[T_0^2+a^2T_0+(7a^4/24)]\kappa^4\}+0(\kappa^8). \quad (63)$$

The fact that our correction term $-\kappa^2k\lambda(k)\tau(k)$ vanishes as $\kappa\to 0$ implies that those roots k_2', k_3', $\cdots$ of Eq. (57) which contribute to the remainder $f(r)$ possess in this limit very large imaginary parts, exactly as do the corresponding roots k_2, k_3, $\cdots$ of the simpler Eq. (55) as shown in Appendix B. Each of the resulting exponential components of $f(r)$ decay rapidly to zero, so $f(r)$ must do the same. The natural presumption must be that $f(r)$ is determined in the last analysis by the rigid ionic cores, and in the dilute electrolyte should therefore be confined in spatial extent to a small multiple of diameter a.

We can implement a crude determination of at least the dominant features of $f(r)$ by using the exact electroneutrality and second-moment conditions on the ion atmosphere [Eqs. (72) and (73) in Paper I]:

$$-1=\frac{4\pi N}{V}\int_a^\infty r^2[g_{+\,+}^{(2)}(r)-g_{+\,-}^{(2)}(r)]\,dr; \quad (64)$$

$$-\frac{6}{\kappa^2}=\frac{4\pi N}{V}\int_a^\infty r^4[g_{+\,+}^{(2)}(r)-g_{+\,-}^{(2)}(r)]\,dr. \quad (65)$$

In view of Eq. (61) these may be interpreted as two integral conditions on $f(r)$; with the aid of development (63), these integral conditions carried to lowest nontrivial orders in κ are quite simple,

$$T_0\kappa^2=\int_a^\infty rf(r)\,dr; \quad (66)$$

$$\tfrac{1}{5}(\kappa^3a^5)=\int_a^\infty r^3f(r)\,dr. \quad (67)$$

The more rapid vanishing with κ of the second of these integrals than the first indicates that $f(r)$ has both positive and negative portions.

Of course $f(r)$ vanishes inside $r=a$, and since it is presumably rather concentrated just outside this collision diameter, we shall suppose that it may be represented by a sum of two Dirac delta functions, one

at a and the other at $2a$:

$$f(r)\cong f_1\delta(r-a-0)+f_2\delta(r-2a). \tag{68}$$

Equations (64) and (65) immediately allow constants f_1 and f_2 to be found,

$$f_1=(4T_0\kappa^2/3a)-(\kappa^3a^2/15),$$
$$f_2=-(T_0\kappa^2/6a)+(\kappa^3a^2/30). \tag{69}$$

Now that at least an approximate determination of the ion-atmosphere charge density is available it is possible to compute the electrostatic free energy of the electrolyte. First it is necessary to find the change in mean electrostatic potential $\Delta\psi_+$ at the center of a cation due to the charge in its diffuse atmosphere. By integrating Poisson's equation we obtain finally

$$\Delta\psi_+(\xi)=(Ze\xi/\epsilon_0)$$
$$[-\kappa\xi+\kappa^2a\xi^2+(7T_0\kappa^2/6a)\xi^2+O(\xi^3\kappa^3)]; \tag{70}$$

here we have quoted the result for ions all partially charged to extent ξ, where $\xi=1$ corresponds to the fully charged ion assembly. The electrostatic free energy per ion, divided by k_BT, equals an integral over ξ giving the reversible isothermal work performed in charging up all ions, minus that for free ions; its form is the following:

$$\frac{Ze}{k_BT}\int_0^1\Delta\psi_+(\xi)\,d\xi=\frac{(Ze)^2}{\epsilon_0k_BTa}$$
$$\times\{-\tfrac{1}{3}(\kappa a)+\tfrac{1}{4}[\kappa^2a^2+\tfrac{7}{6}(T_0\kappa^2)]+O(\kappa^3)\}. \tag{71}$$

In order to assess the character of the term containing T_0 in free energy (71), we pass to the limit of zero concentration. In that case the ion-pair size distribution function $p^{(1)}(s)$ in definition (58) of T_0 becomes very long-ranged relative to sphere diameter a, so we may write

$$T_0\sim-a^3P_3/3P_4, \tag{72}$$

where the P_n are the moments of $p^{(1)}(s)$,

$$P_n=\int_0^\infty s^np^{(1)}(s)\,ds. \tag{73}$$

Indeed it is valid in this low-concentration case simply to take $p^{(1)}$ to be the ideal-gas function scrutinized in Sec. II. Analytic approximation (15) thereupon leads to an explicit value for T_0,

$$T_0\cong-(a^3/3)(\pi N/6V)^{1/3}. \tag{74}$$

In Paper I the excess Helmholtz free energy per ion, divided by k_BT, was denoted by $F_1(\zeta_1,\zeta_2)$, where the two dimensionless parameters ζ_1 and ζ_2 characterizing the interactions were defined by the relations

$$\zeta_1=2Na^3/V,$$
$$\zeta_2=(Ze)^2/\epsilon_0ak_BT. \tag{75}$$

The electrical charging work shown in Eq. (71), along with expression (74) for T_0, leads to the following prediction:

$$F_1(\zeta_1,\zeta_2)=F_1(\zeta_1,0)-\tfrac{2}{3}(\pi\zeta_1)^{1/2}\zeta_2^{3/2}$$
$$+\pi\zeta_1\zeta_2^2-\tfrac{7}{24}(\tfrac{2}{3}\pi\zeta_1)^{4/3}\zeta_2^2+\cdots. \tag{76}$$

The first term in the right hand member is the excess free energy for uncharged rigid cores, and it is followed by the well-known Debye–Hückel term varying as the square root of concentration. The third term (also predicted by the standard Debye–Hückel theory with ion size a taken into account) arises physically from outward displacement of the ion atmosphere by diameter a, but still presuming the relevant decay constant is κ exactly. The last term shown varies as the four-thirds power of concentration, and appears to have no precedent in other electrolyte theories heretofore advanced. The terms not shown in Eq. (76) will either contain higher powers of ζ_2 than the second, or if they are proportional to ζ_2^2 will have ζ_1 to a power exceeding four-thirds.

VII. DISCUSSION

The crude delta-function distribution imputed to $f(r)$ is of course unrealistically sharp, and should be viewed in a "smeared" sense. Since f_1 is negative and f_2 positive, we may infer that the magnitude of the ion atmosphere charge density is actually a bit greater just beyond $r=a$ compared to the contribution of the single longest-ranged exponential component, and then around $r=2a$ the magnitude is less. The situation is illustrated pictorially in Fig. 7. The resultant ion-atmosphere charge density seems very much to be in the process of developing regions of opposite charge sign, which was shown in Paper I necessarily to obtain when $\kappa a>6^{1/2}$.

The mean activity coefficient $\gamma_\pm$ is readily obtainable

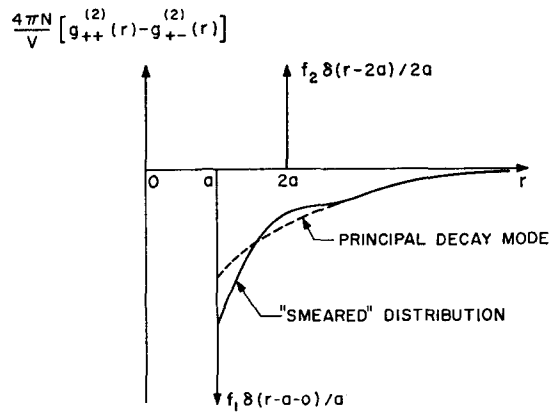

FIG. 7. Components of the ion-atmosphere charge density. The principal decay mode corresponds to the single exponential decay remaining in the Debye–Hückel limit. The crude two-delta-function approximation to the remainder, Eq. (68), has been added to the principal mode in a more realistic "smeared" sense.

from the excess free energy $F_1(\zeta_1, \zeta_2)$:

$$\begin{aligned}\ln\gamma_\pm &= F_1(\zeta_1,\zeta_2)+\zeta_1[\partial F_1(\zeta_1,\zeta_2)/\partial\zeta_1] \\ &= \{F_1(\zeta_1,0)+\zeta_1[\partial F_1(\zeta_1,0)/\partial\zeta_1]\} \\ &\quad -(\pi\zeta_1)^{1/2}\zeta_2^{3/2}+2\pi\zeta_1\zeta_2^2-\tfrac{4}{7}\tfrac{9}{2}(\tfrac{2}{3}\pi\zeta_1)^{4/3}\zeta_2^2+\cdots . \end{aligned} \tag{77}$$

The contribution enclosed in braces arises purely from the hard-sphere interactions, and would be present even if all ions were discharged:

$$\begin{aligned}&\{F_1(\zeta_1,0)+\zeta_1[\partial F(\zeta_1,0)/\partial F_1]\} \\ &\quad =\tfrac{4}{3}\pi\zeta_1+(5\pi^2/12)\zeta_1^2+3.5150\zeta_1^3+O(\zeta_1^4). \end{aligned} \tag{78}$$

Although the approximations we were forced to make render the numerical coefficient of the last term in Eq. (77) a mere estimate, the sign and order of magnitude are still probably correct.

The occurrence of third-integral powers of concentration (ζ_1) in the free energy or activity coefficient arises quite naturally in the present theory as the distance scaling for the mean separation of ion pairs. Whereas the earlier theoretical descriptions[2–4,13] of concentrated electrolytes have computed the distribution of *single* ions in a self-consistent average field set up either by a charged electrode or a fixed ion, we have gone a step further and attempted self-consistent description of *pairs*. Not only does this present more elaborate treatment generate the $-\kappa^2 k\lambda(k)\tau(k)$ correction (which is the source of the $\zeta_1^{4/3}$ dependence in free energy), but it also utilizes for the first time the exact second-moment condition (65).

In many ways we have only "scratched the surface" in the possible uses of the ion-pair theory. This general approach in fact seems well suited to description of very concentrated electrolytes and molten salts, since it may be set up as a variational problem. The reduced excess free energy F_1 may be written as a functional of the ion-pair size distribution,

$$F_1[p^{(1)}]=F_{\mathrm{HS}}[p^{(1)}]+F_c[p^{(1)}]. \tag{79}$$

The first part F_{HS} is the free-energy functional just for the uncharged hard-sphere ion cores, and was exhibited in Paper I, Eq. (19), as a cluster series. The electrical charging work F_c corresponds to Eq. (71) above, and through the function $\epsilon(k)$ obviously depends on $p^{(1)}$. The correct free energy and size distribution will then correspond to minimization of functional (79) under suitable restraints.

In principle our ion-pair theory could be extended to unsymmetrical electrolytes by definition of uncharged complexes of ions containing necessarily more than just a pair of ions. Furthermore, the general procedure should also be adaptable to description of electrical double layers at phase boundaries. However each of these projects pose special problems that we leave for future investigation.

APPENDIX A

The pair correlation function $g_{+-}^{(2)}(r)$ in the ideal binary-gas mixture considered in Sec. II is identically unity, reflecting absence of forces. A + and a − particle separated by the requisite distance r may or may not belong to the same "ion" pair, so we write

$$\left(\frac{N}{V}\right)^2 g_{+-}^{(2)}(r)=p^{(1)}(r)+\int d\mathbf{s}_1\int d\mathbf{s}_2 \times p^{(2)}[\mathbf{s}_1,\tfrac{1}{2}(\mathbf{s}_1+\mathbf{s}_2)-\mathbf{r},\mathbf{s}_2]. \tag{A1}$$

The arguments $\mathbf{s}_1$ and $\mathbf{s}_2$ as shown in Fig. 8 are the − to + separations of the two pairs involved in doublet probability $p^{(2)}$, and $\frac{1}{2}(\mathbf{s}_1+\mathbf{s}_2)-\mathbf{r}$ connects their centers.

We approximate $p^{(2)}$ appearing in Eq. (A1) by a product of $p^{(1)}$'s, times a Boltzmann factor for the steric-hindrance potential u acting between the pairs:

$$\left(\frac{N}{V}\right)^2 = p^{(1)}(r)+\int d\mathbf{s}_1\int d\mathbf{s}_2 p^{(1)}(s_1)p^{(1)}(s_2) \times \exp\{-\beta u[\mathbf{s}_1,\tfrac{1}{2}(\mathbf{s}_1+\mathbf{s}_2)-\mathbf{r},\mathbf{s}_2]\}. \tag{A2}$$

In view of the normalization condition (28) on $p^{(1)}$, this last equation may be rewritten

$$p^{(1)}(r)=\int d\mathbf{s}_1\int d\mathbf{s}_2 p^{(1)}(s_1)p^{(1)}(s_2) \times(1-\exp\{-\beta u[\mathbf{s}_1,\tfrac{1}{2}(\mathbf{s}_1+\mathbf{s}_2)-\mathbf{r},\mathbf{s}_2]\}). \tag{A3}$$

The quantity in bold parentheses has only values 1 or 0, depending on whether or not the pairs overlap.

Define K to be the angular average of the quantity enclosed in bold parentheses in Eq. (A3), over directions of both $\mathbf{s}_1$ and $\mathbf{s}_2$, at fixed r, s_1, and s_2:

$$K\left(\frac{s_1}{r},\frac{s_2}{r}\right)=(4\pi)^{-2}\int d\Omega_1\int d\Omega_2 (1-\exp\{-\beta u[\mathbf{s}_1,\tfrac{1}{2}(\mathbf{s}_1+\mathbf{s}_2)-\mathbf{r},\mathbf{s}_2]\}). \tag{A4}$$

As shown, we can take this quantity to depend only on distances reduced by r, for if each of s_1, s_2, and r are doubled, for instance, the fractional overlap K remains unchanged. Integral Eq. (A3) thus simplifies to the following:

$$p^{(1)}(r)=\int_0^\infty 4\pi s_1^2 ds_1\int_0^\infty 4\pi s_2^2 ds_2 \times p^{(1)}(s_1)p^{(1)}(s_2)K\left(\frac{s_1}{r},\frac{s_2}{r}\right). \tag{A5}$$

When distance r is very large, K will be zero or negligibly small unless both s_1 and s_2 are also large. Therefore we test the algebraic tail asymptote

$$p^{(1)}(r)\sim(l'/r)^{n'} \tag{A6}$$

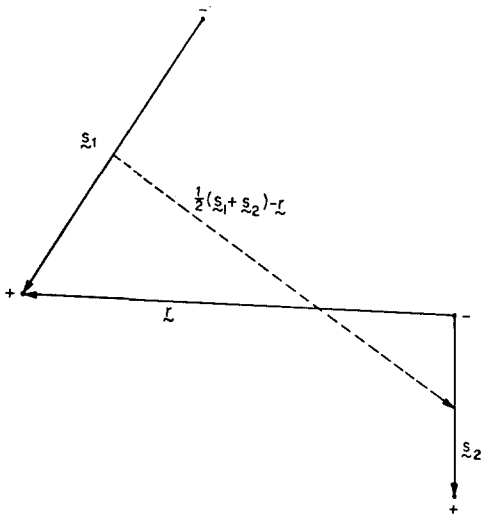

FIG. 8. Vector variables describing simultaneous configurations of two pairs, separations s_1 and s_2, used in Eq. (A1).

by direct substitution into Eq. (A5),

$$\left(\frac{l'}{r}\right)^{n'} = \int_0^\infty 4\pi s_1^2 ds_1 \int_0^\infty 4\pi s_2^2 ds_2 \left(\frac{l'}{s_1}\right)^{n'} \left(\frac{l'}{s_2}\right)^{n'} K\left(\frac{s_1}{r}, \frac{s_2}{r}\right)$$

$$= 16\pi^2 (l')^{2n'} r^{6-2n'} \int_0^\infty dx_1 \int_0^\infty dx_2 (x_1 x_2)^2 K(x_1, x_2). \tag{A7}$$

The double integral is a pure number, independent of r. Consistency requires in Eq. (A7) that exponents of r on both sides be equal,

$$-n' = 6 - 2n',$$

$$n' = 6. \tag{A8}$$

This is the same exponent prediction as achieved in Sec. II.

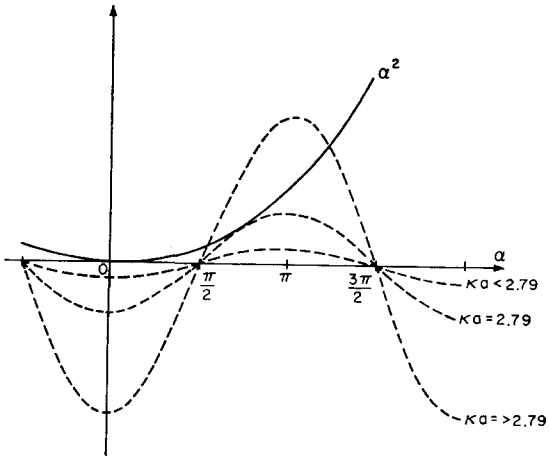

FIG. 9. Graphical solution of Eq. (B8). The family of dotted curves are $-(\kappa a)^2 \cos\alpha$ for various κa.

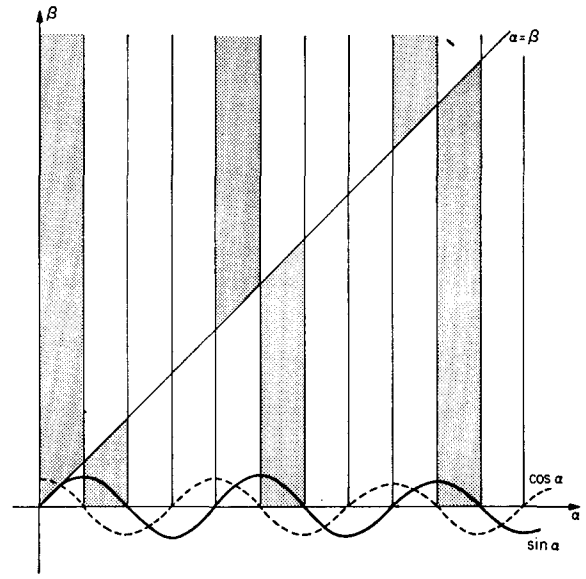

FIG. 10. Regions (shaded) for which solutions to Eqs. (B2) and (B3) are possible.

APPENDIX B

We wish to examine the roots of the transcendental equation (55) in the complex-k plane. Set $z=ka$, so

$$z^2 + (\kappa a)^2 \cos z = 0. \tag{B1}$$

If $z=\alpha+i\beta$, the real and imaginary parts of Eq. (B1) separately constitute transcendental equations, which are coupled to one another:

$$\beta^2 - \alpha^2 = (\kappa a)^2 \cos\alpha \cosh\beta; \tag{B2}$$

$$2\alpha\beta = (\kappa a)^2 \sin\alpha \sinh\beta. \tag{B3}$$

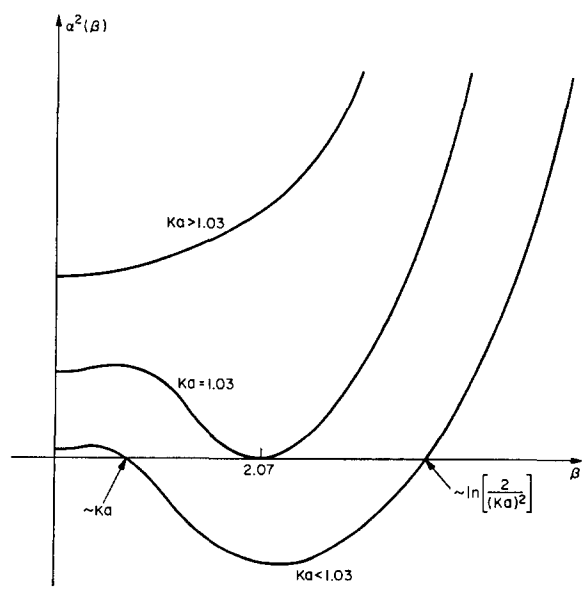

FIG. 11. Schematic plot of $\alpha^2(\beta)$ defined by Eq. (B14). The axis intersections shown for the $\kappa a < 1.03$ curve are the small-κa asymptotes given in Eqs. (B5) and (B7).

It is clear that if the pair (α, β) satisfy these coupled equations, so also do $(-\alpha, \beta)$, $(\alpha, -\beta)$, and $(-\alpha, -\beta)$. A solution in any one of the four quadrants is thus replicated in the other three by reflection across the axes.

We first examine the possibility of pure imaginary solutions, for which (B3) collapses and (B2) reduces to

$$\beta^2 = (\kappa a)^2 \cosh\beta. \tag{B4}$$

For sufficiently small κa it is easy to see that a graphical plot of the two members of Eq. (B4) will intersect four times, twice near the origin [because the parabolic left member increases much faster initially than the right member with its small $(\kappa a)^2$ factor], and twice far from the origin [since for large $|\beta|$ the exponential behavior of cosh β will overcome $(\kappa a)^2$]. For the smaller pair, a straightforward iteration yields[14]

$$z = \pm i\kappa a\{1+\tfrac{1}{4}(\kappa a)^2+\tfrac{1}{96}(\kappa a)^4+\tfrac{379}{57600}(\kappa a)^6+O[(\kappa a)^8]\}. \tag{B5}$$

In order to find the larger pair, Eq. (B4) may first be rewritten

$$\beta = \pm\left\{\ln\left[\frac{2}{(\kappa a)^2}\right]+\ln\left[\frac{\beta^2}{1+\exp(-2|\beta|)}\right]\right\}, \tag{B6}$$

and then iterated, for small κa,

$$z = i\beta \sim \pm i\left\{\ln\left[\frac{2}{(\kappa a)^2}\right]+2\ln\ln\left[\frac{2}{(\kappa a)^2}\right]+\frac{4\ln\ln[2/(\kappa a)^2]}{\ln[2/(\kappa a)^2]}+\cdots\right\}. \tag{B7}$$

Numerical studies show[2,3] that as κa increases from zero, the roots (B5) and (B7) approach each other in pairs, and coalesce at $\kappa a = 1.03$. Thereafter, they move off the imaginary axis.

Pure real solutions must satisfy

$$\alpha^2 = -(\kappa a)^2 \cos\alpha. \tag{B8}$$

As Fig. 9 shows, the curves α^2 and $-(\kappa a)^2\cos\alpha$ do not intersect when $\kappa a < 2.79$. When $\kappa a = 2.79$ the curves are tangent to each other indicating a pair of double roots. As κa increases beyond 2.79 these roots separate (the curves cross), and thereafter at regular intervals further crossings continue to appear and persist as the amplitude of the cosine curve continues to increase. In the large-κa limit the roots of (B8) will occur at

$$\pm\tfrac{1}{2}\pi, \quad \pm\tfrac{3}{2}\pi, \quad \pm\tfrac{5}{2}\pi, \cdots, \tag{B9}$$

out to $|\alpha| \cong \kappa a$.

The remaining solutions correspond to points in the first quadrant with $\alpha > 0$, $\beta > 0$. Equation (B3) allows

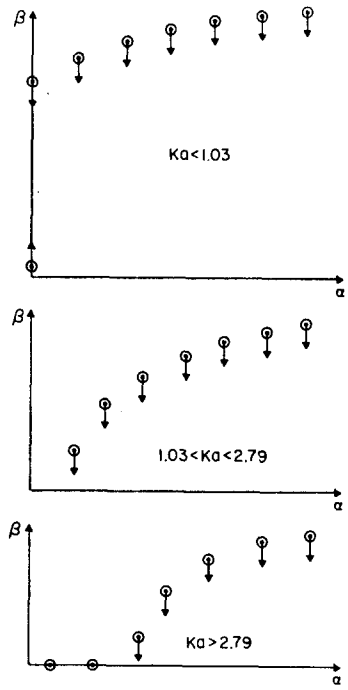

FIG. 13. Position of transcendental equation zeros in the first quadrant. The small arrows indicate roughly the direction of motion as κa increases.

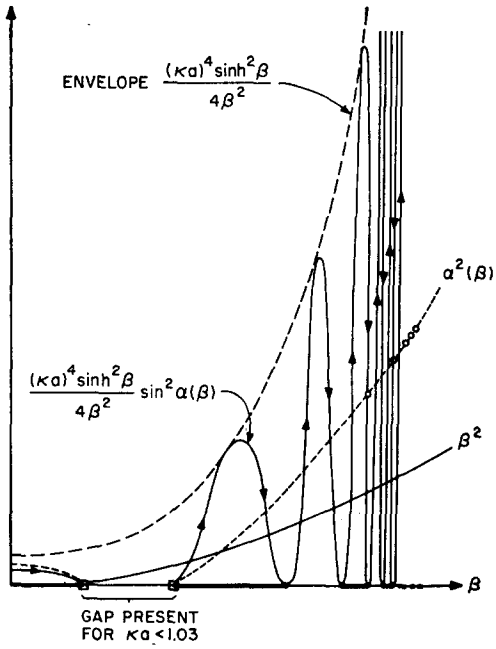

FIG. 12. Plot of the two members, $\alpha^2(\beta)$ and $(\kappa a)^4\sinh^2\beta\times\sin^2\alpha(\beta)/4\beta^2$, of Eq. (B18). Although the curves cross many times, only those crossings satisfying (B10) and (B11) qualify as solutions to the basic pair of transcendental Eqs. (B2) and (B3), and they are denoted by circles. As explained in the text, these solutions must have β in the heavily shaded intervals, and be on ascending or descending portions of the directed curve, respectively, if they are below or above the β^2 parabola. The curves have been drawn presuming $\kappa a < 1.03$, for which the little squares on the β axis locate the two pure imaginary solutions (B5) and (B7).

[14] The root with the upper sign is the one instrumental in recovery of the Debye–Hückel theory at low concentration. The numerical coefficient of the $(\kappa a)^6$ term shown here was incorrectly quoted in Ref. 3.

us to conclude that $\sin\alpha>0$, or equivalently

$$2n\pi<\alpha<(2n+1)\pi \qquad (n=0, 1, 2, 3, \cdots). \tag{B10}$$

Furthermore we see from Eq. (B2) that

$$\begin{aligned} &\beta>\alpha \qquad \text{if } \cos\alpha>0, \\ &\beta<\alpha, \qquad \text{if } \cos\alpha<0. \end{aligned} \tag{B11}$$

Figure 10 displays the regions allowed by conditions (B10) and (B11) in the α,β plane, in the form of shaded strips.

If both Eqs. (B2) and (B3) are squared, the trigonometric functions of α may be eliminated, with the result

$$\alpha^4+(4\beta^2\coth^2\beta-2\beta^2)\alpha^2+\beta^4-(\kappa a)^4\cosh^2\beta=0. \tag{B12}$$

Solve for α^2,

$$\alpha^2=\beta^2-2\beta^2\coth^2\beta \pm\{[2\beta^2\coth^2\beta-\beta^2]^2+(\kappa a)^4\cosh^2\beta-\beta^4\}^{1/2}. \tag{B13}$$

Since $\beta^2-2\beta^2\coth^2\beta<0$ for all positive β, we are compelled to take the upper sign,

$$\alpha^2=\{[2\beta^2\coth^2\beta-\beta^2]^2-\beta^4+(\kappa a)^4\cosh^2\beta\}^{1/2} -2\beta^2\coth^2\beta+\beta^2. \tag{B14}$$

Obviously we can consider only those positive β values which render the last expression positive. The sign of its right member is the same as the sign of

$$(\kappa a)^4\cosh^2\beta-\beta^4=[(\kappa a)^2\cosh\beta+\beta^2] \times[(\kappa a)^2\cosh\beta-\beta^2], \tag{B15}$$

and is thus the same as $(\kappa a)^2\cosh\beta-\beta^2$. In the light of Eq. (B4) we see that for $\kappa a<1.03$, there will be an interval of β values which is excluded, but when $\kappa a>1.03$ the entire set of positive β's will be allowed. Figure 11 provides a schematic diagram of the function $\alpha^2(\beta)$ defined by Eq. (B14). Near the origin

$$\alpha^2(\beta)\sim 2\{[1+\tfrac{1}{4}(\kappa a)^4]^{1/2}-1\}+O(\beta^2), \tag{B16}$$

and for large β,

$$\alpha^2(\beta)\sim\tfrac{1}{2}(\kappa a)^2\exp(\beta). \tag{B17}$$

Equation (B3) may be put into the following form:

$$a^2(\beta)=[(\kappa a)^4\sinh^2\beta/4\beta^2]\sin^2\alpha(\beta). \tag{B18}$$

The eventual rapid increase of $\alpha(\beta)$ as β gets large means that $\sin^2\alpha(\beta)$ will oscillate between 0 and 1 faster and faster. The amplitude modulating factor $(\kappa a)^4\sinh^2\beta/4\beta^2$ in Eq. (B18) then provides an envelope for these rapid oscillations, which itself increases in height essentially as $\exp(2\beta)$ at large β. Since Eq. (B17) indicates a slower divergence for the left member of (B18), the curves of the two members will continue to intersect an infinite number of times, as shown qualitatively in Fig. 12.

The curve for the right member of (B18) has been given a direction by means of arrows. Valid solutions to the original pair (B2) and (B3) can occur first only in vertical strips indicated by the heavy interval lines along the β axis [these are the graphical statement of (B10)]. Secondly, condition (B11) demands that if an intersection of the curves for the left and right members of (B18) occurs on an *ascending* part of the latter, it must also be *below* the β^2 parabola, or if on a *descending* part it must be *above* the β^2 parabola. It is clear from the figure that eventually the roots will occur on every other descent, and the asymptotic character of the roots will be

$$\begin{aligned} &\alpha_n\sim(2n+1)\pi, \\ &\beta_n\sim\ln[2\pi^2(2n+1)^2/(\kappa a)^2]. \end{aligned} \tag{B19}$$

The infinite set of solutions (B19) in the complex-z plane (i.e., the α,β plane) is essentially evenly spaced along a logarithmic curve, since

$$\beta_n\sim\ln[2\alpha_n^2/(\kappa a)^2], \tag{B20}$$

whose starting point is farther and farther up the imaginary β axis as $\kappa a\to 0$.

In the final Fig. 13 we have assembled in pictorial form the behavior of the roots to Eq. (B1) in the first quadrant as κa increases. The two pure imaginary roots move toward one another when $\kappa a<1.03$, while the remainder along the logarithmic branch (B20) move downward, essentially all at about the same rate. After the two pure imaginaries merge and move off the axis (one into the second quadrant), the entire set of roots continue their descent onto the real (α) axis, where one by one they stick at positions (B9).